Reentry Trajectory Design with Pigeon Inspired Optimization Using Derived Angle of Attack Profile

Gangireddy Sushnigdha[1] and Ashok Joshi[2]

Abstract: This paper proposes two strategies that generate the entry trajectories using pigeon inspired optimization (PIO) for a lifting type reentry vehicle. The obtained entry trajectory should be within the entry corridor formed by the specified upper bounds on heat rate, dynamic pressure, and load factor. In both the approaches, bank angle which is parametrized to be a linear function of energy and angle of attack are considered as the control variables. This paper presents a methodology that converts the path constraints to allowable bounds on the angle of attack. The angle of attack at any instant is obtained by using the load factor constraint in the first approach and in the second approach, the angle of attack is obtained using the heat rate and load factor constraints. Hence, the path constraints are satisfied by modulating the angle of attack alone. In both cases, bank angle is suitably modulated to achieve the desired terminal range-to-go and also to maintain the equilibrium glide condition. The terminal heading angle offset is minimized using traditional bank reversal logic. These two scrategies are simulated for common aero vehicle (CAV-H) with a high lift to drag (L/D) ratio. Simulation results show that the entry trajectories obtained using the PIO algorithm have satisfied the path constraints and achieved the terminal range-to-go accurately. **DOI: 10.1061/(ASCE)AS.1943-5525.0000929.**

Introduction

The reentry phase is very crucial for any spacecraft, reusable launch vehicle, and hypersonic gliding vehicles, that are returning from the space to the Earth. The common aero vehicle (CAV-H) is a hypersonic glide vehicle with a high lift to drag ratio of 3.5; this feature enables this vehicle to travel more than 10,000 km. The reentry phase is the longest and most critical phase of the CAV-H. The vehicle is unpowered in this phase, and, therefore, the trajectory is governed by only gravity and aerodynamic forces. The energy dissipation in this phase has to be carried out in a controlled way to maintain the thermal load factor and dynamic pressure constraints within the specified limits. This is achieved by modulating the bank angle and/or angle of attack.

Entry vehicles rely on entry trajectories which are designed using trajectory optimization techniques to reach the destination safely. Designing the entry trajectories for the CAV-H is a challenging task because it has highly nonlinear entry dynamics, longer duration of reentry phase, and its entry trajectory exhibits oscillations which increase the integrated thermal and g-loads experienced by the vehicle.

Designing entry trajectory for re-entry vehicles is basically an optimal control problem whose solution is obtained numerically through indirect or direct methods. Indirect methods are based on the Pontryagin's minimum principle (Pontryagin and Boltyanskii 1962) which leads to a two-point boundary value problem, whose solution process involves choosing initial guesses for the costate variables which is nonintuitive. On the other hand, direct methods are based on discretizing control and/or state variable time histories, and, thereby, transforming the optimal control problem to a nonlinear programming problem (NLP) which is relatively easier to solve. The pseudospectral methods that fall under the category of direct methods are used extensively to solve the trajectory optimization problems. Tian and Qun Zong (Bailing and Qun 2011) have implemented the Legendre pseudospectral approach for solving the entry trajectory optimization problem. The Chebyshev pseudospectral method is applied for generating entry trajectories by Wei (Cai et al. 2015). However, the basis functions and the number of collocation points have to be selected carefully to avoid tuning issues in these methods. The pseudospectral methods are also reported to be sensitive to initial-guess values of the control and state variables (Su and Wang 2015). A new approach for trajectory optimization called model predictive static programming which combines the philosophies of model predictive control and approximate dynamic programming is brought into the framework of guidance in Halbe et al. (2014). Unlike the two-point boundary value problems, this approach demands a static costate vector for updating the control history and is proven to be computationally efficient for solving the reentry guidance problem. Another promising approach for solving the entry trajectory optimization problem is proposed by Liu et al. (2016) which uses second-order cone programming (SOCP). This SOCP problem is solved efficiently and reliably by interior-point methods, which have only polynomial complexity and do not require user-defined initial guesses. However, this approach requires considerable efforts to reformulate the original problem into the framework of SOCP.

The metaheuristic algorithms fall under the category of direct methods that mimic natural phenomena. They have gained popularity because they have a simple solution mechanism without involving calculations of derivatives; they are flexible and can be applied to various optimization problems pertaining to any domain. Few metaheuristic algorithms are population driven algorithms; they have the capacity to avoid falling into the trap of a local optimal solution. Some of the population-based metaheuristic algorithms are particle swarm optimization (PSO), PIO, and genetic algorithm (GA).

[1]Research Scholar, Dept. of Aerospace Engineering, Indian Institute of Technology Bombay, Mumbai, Maharashtra 400076, India (corresponding author). Email: sushnigdha.g@gmail.com

[2]Professor, Dept. of Aerospace Engineering, Indian Institute of Technology Bombay, Mumbai, Maharashtra 400076, India. Email: ashokj@aero.iitb.ac.in

Note. This manuscript was submitted on January 12, 2018; approved on May 8, 2018; published online on August 23, 2018. Discussion period open until January 23, 2019; separate discussions must be submitted for individual papers. This paper is part of the ***Journal of Aerospace Engineering***, © ASCE, ISSN 0893-1321.

Optimal trajectories for a spacecraft are generated using PSO in Rahimi et al. (2013). To overcome the issue of premature convergence in the PSO algorithm, a stochastic gradient-based particle swarm optimization is proposed in Li et al. (2018). Stochastic gradient is calculated using the best positions in two adjacent iterations. This method is applied to solve the entry trajectory optimization problem by considering both angle of attack and bank angle as the control variables. Artificial bee colony-based entry trajectory optimization for the hypersonic vehicle is carried out in Duan and Li (2015) where bank angle is considered to be the only control variable. Naresh Kumar et al. (2018) has implemented a pattern search algorithm for finding control variables that maximize the range travelled by a hypersonic boost glide vehicle in Naresh Kumar et al. (2018) and an additional constraint on minimum dynamic pressure is considered to ensure controllability of the vehicles at higher altitudes. In recent times, a metaheuristic algorithm named PIO that mimics the homing behavior of pigeons is proposed by Duan and Qjao (2014). Pigeons have special ability to sense the magnetic field of the Earth and identify the altitude of the Sun. They can identify landmarks near the destination. They use these special abilities to reach the destination. Zhao and Zhou (2015a, b) have implemented PSO and PIO to generate entry trajectories for a hypersonic gliding vehicle using a simple formulation. However, the control formulation requires finding multiple parameters to get the complete control profile. The PIO algorithm is used to generate the entry trajectory for the CAV-H vehicle in Sushnigdha and Joshi (2017) with only bank angle as the control variable. It is observed that convergence of the PIO is faster than the PSO and gravitational search algorithms (GSA).

In the literature Lu (2014) and Zhao and Zhou (2015a, b), researchers have formulated entry guidance and trajectory optimization algorithms using a nominal angle of attack profile for CAV-H and have considered the bank angle to be the only control variable which is to be modulated to satisfy path and terminal conditions. In general, the nominal angle of attack profile is chosen based on the occurrence of maximum L/D so as to maximize the downrange capabilities of the vehicle; this profile might not allow the entry trajectory to satisfy the heat rate constraint. This leads to the requirement of modulating the bank angle for satisfying the path and terminal constraints. In Li et al. (2015), all path constraints are converted to limits on the angle of attack, which forces the angle of attack commands to be within these limits. The path constraints are first converted to limits on altitude, using bounds on the angle of attack that are contained in Zhu et al. (2015).

This paper presents a trajectory optimization algorithm based on PIO where both the angle of attack and bank angle are the control variables. Two cases that differ in the methodology of generating angle of attack commands are discussed. In both the cases, the bank angle that minimizes the terminal range-to-go error is obtained using the PIO algorithm. This bank angle is further modified to satisfy the equilibrium glide condition, while the angle of attack commands are derived using the given path constraints, and it is modulated accordingly to satisfy them. In the first case, the angle of attack is obtained using only the load factor constraint. In the second case, the angle of attack is initially derived from the heat rate constraint and subsequently when the vehicle attains a specified Mach number $Mach_{shift}$, the angle of attack commands are derived from the load factor constraint.

Mathematical Model for Reentry Vehicle

This section introduces the gliding vehicle CAV-H which is used for the simulations and describes its equations of motion. It also gives the details of gravity, atmospheric models, and terminal and path constraints that are considered for simulations.

The common aero vehicle (CAV) is a concept which describes a space reentry aeroshell launched into space on a suitable vehicle, which then survives atmospheric re-entry, reduces its speed to low Mach numbers and dispenses a cargo, payload, or weapons in the atmosphere of the Earth (Phillips 2003). In this paper, CAV with a high L/D ratio (CAV-H) is used for simulations.

Equations of Motion

The entry vehicle is considered to be a point mass, gliding over a spherical rotating Earth. Its equations of motion in terms of nondimensional variables are given as follows (Lu 2014)

$$\dot{r} = V \sin\gamma \tag{1}$$

$$\dot{V} = -D - \left(\frac{\sin\gamma}{r^2}\right) + \Omega^2 r \cos\phi(\sin\gamma\cos\phi - \cos\gamma\sin\phi\cos\psi) \tag{2}$$

$$\dot{\theta} = \frac{V\cos\gamma\sin\psi}{r\cos\phi} \tag{3}$$

$$\dot{\phi} = \frac{V\cos\gamma\cos\psi}{r} \tag{4}$$

$$\dot{\gamma} = \frac{1}{V}\left[L\cos\sigma + \left(V^2 - \frac{1}{r}\right)\left(\frac{\cos\gamma}{r}\right) + 2\,\Omega V\cos\phi\sin\psi + \Omega^2 r\cos\phi(\cos\gamma\cos\phi + \sin\gamma\cos\psi\sin\phi)\right] \tag{5}$$

$$\dot{\psi} = \frac{1}{V}\left[\frac{L\sin\sigma}{\cos\gamma} + \frac{V^2}{r}\cos\gamma\sin\psi\tan\phi - 2\,\Omega V(\tan\gamma\cos\psi\cos\phi - \sin\phi) + \frac{\Omega^2 r}{\cos\gamma}\sin\psi\sin\phi\cos\phi\right] \tag{6}$$

$$\dot{s} = -V\cos\gamma/r \tag{7}$$

In the literature (Vinh et al. 1980), all the variables in equations of motion are presented in dimensionless form to make them applicable to any vehicle regardless of its weight, shape, and size, entering an arbitrary planetary atmosphere. Therefore, all the variables in the above- mentioned equations of motion are nondimensional, and the derivatives are with respect to the dimensionless time τ. The dimensional time t is obtained using $t = \tau t_{\text{scale}}$, where $t_{scale} = \sqrt{\frac{R_0}{g_0}}$. R_0 = radius of Earth, g_0 = acceleration due to gravity on the surface of the Earth. r = nondimensional distance from the Earth center to the point mass, O, that is normalized by the radius of the Earth $R_0 = 6{,}378.135$ km. Normalized radial distance and normalized time results in the normalized Earth-relative velocity V which is nondimensional, and the normalizing factor is $V_{scale} = \sqrt{R_0 g_0}$. Longitude and latitude are denoted by θ and ϕ, respectively. The flight-path angle γ is positive when V is above the horizontal plane. ψ is the heading angle of the velocity vector, measured clockwise in the local horizontal plane from the north as shown in Fig. 1. The range-to-go s (in radians, normalized by R_0) on the surface of the spherical Earth along the great circle connecting the current location of the vehicle and the site of the final destination (Lu 2014). σ is the bank angle which is defined as clockwise positive rotation of the lift vector about the velocity vector. The dimensionless angular velocity of the Earth is denoted by Ω. L and D are

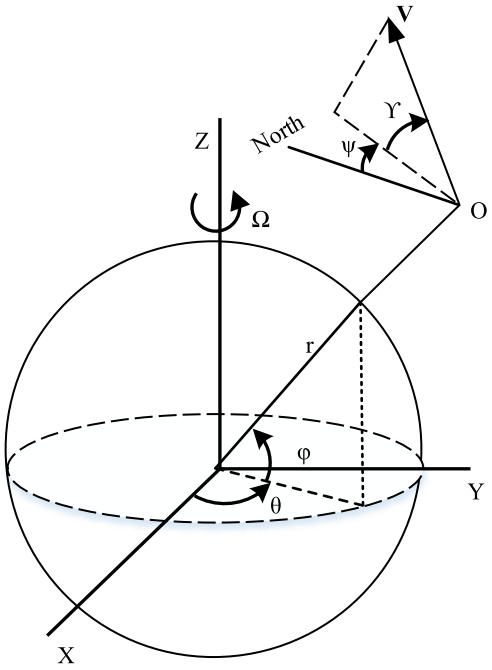

Fig. 1. Nomenclature used in the equations of motion. (Reprinted from *Engineering Applications of Artificial Intelligence*, 69, G. Sushnigdha and A. Joshi, "Evolutionary Method Based Integrated Guidance Strategy for Reentry Vehicles," 168–177, Copyright 2018, with permission from Elsevier.)

nondimensional aerodynamic lift and drag accelerations, respectively, normalized with $g_0 = 9.8$ m/s^2 and are defined as

$$L = \frac{1}{2mg_0}\rho V^2 C_L S_{ref} \tag{8}$$

$$D = \frac{1}{2mg_0}\rho V^2 C_D S_{ref} \tag{9}$$

where m = mass of the vehicle, S_{ref} = surface area of the wing, ρ = atmospheric density. C_L and C_D = aerodynamic lift and drag coefficients, respectively, that are functions of angle of attack and Mach number. For the CAV-H vehicle, the aerodynamic coefficient details are given in Phillips (2003).

Independent Variable and Calculation of Final Time of Flight t_f

An energy like variable e defined as the negative of the specific mechanical energy used in orbital mechanics is considered as the independent variable for solving the trajectory optimization problem (Lu 2014)

$$e = \frac{\mu}{r} - \frac{V^2}{2} \tag{10}$$

$$\dot{e} = DV \tag{11}$$

where μ = gravitational parameter of the Earth, whose normalized value is 1. Eq. (11) shows that e is a monotonically increasing variable and is a function of radial distance and velocity. Therefore, the choice of e as an independent variable helps in considering the terminal conditions on r and V as a single constraint. The equations of motion are rewritten considering e as an independent variable using Eq. (11) as $dr/de = \dot{r}/\dot{e}$. The equations of motion are integrated from initial energy e_0 to final energy e_f. e_0 and e_f are calculated using the initial and desired values of radial distances r_i, r^* and velocities V_i, V^* respectively. The final time of flight t_f is obtained as part of the solution by including $\frac{dt}{de}$ in the equations of motion and integrating it from e_0 to e_f. The order of the system is reduced by eliminating Eq. (2) while integrating the equations of motion. By knowing r and e, velocity V is calculated using Eq. (10).

Gravity and Atmosphere Models

The acceleration due to gravity of the vehicle at a radial distance r from the center of the Earth is given by Eq. (12)

$$g = \frac{\mu}{r^2} \tag{12}$$

The nondimensional value of gravitational parameter μ is 1. This gravity model is considered in describing the equations of motion. The U.S. Standard Atmosphere, 1976 is used to model the atmospheric density (Anon 1976).

Path Constraints

In the entry phase, the vehicle has to travel within the entry corridor formed by the specified upper limits on heat rate $\dot{Q}_{max}$, load factor a_{max}, and dynamic pressure q_{max}. These path constraints are given by Eqs. (13)–(15)

$$\dot{Q} = 9.4369 \times 10^{-5}\sqrt{\rho}V^{3.15}V_{scale}^{3.15} \le \dot{Q}_{max} \tag{13}$$

$$a = \sqrt{L^2 + D^2} \le a_{max} \tag{14}$$

$$q = \frac{\rho V^2 V_{scale}^2}{2} \le q_{max} \tag{15}$$

These path constraints are to be strictly satisfied. There is another soft constraint called the equilibrium glide constraint. Entry vehicles like CAV-H with a high L/D ratio exhibit oscillations in their altitude profiles. These oscillations can be removed when the vehicle is made to satisfy the equilibrium glide constraint. Equilibrium glide refers to the case where the aerodynamic lift force balances the gravitational and centrifugal forces as given in Eq. (16). This equation is obtained by making the derivative of the flight-path angle zero and neglecting the Earth rotation terms

$$L\cos\sigma = (1/r^2) - (V^2/r) \tag{16}$$

In the equilibrium glide condition, the flight-path angle should ideally be constant. However, it is slightly varying. Hence, it is termed the quasi equilibrium glide condition (QEGC) by Lu (2006). In this paper, heat rate and load factor constraints are considered explicitly. The constraint on dynamic pressure is implicitly satisfied by satisfying the load factor constraint.

Terminal Constraints

At the end of the entry phase, the vehicle has to achieve a radial distance r^*, range-to-go s^*, and velocity V^* as per the requirement of the terminal area energy management (TAEM) phase. The heading angle offset $\Delta\psi_f$ at the end of the entry phase should be less than the desired heading angle offset $\Delta\psi_d^*$. This constraint is achieved using traditional bank reversal logic.

Trajectory Optimization Problem

Trajectory optimization of an entry vehicle involves finding the control profiles such that the resulting entry trajectory satisfies the path and terminal conditions. Two cases with both bank angle and angle of attack as the control variables are discussed in this paper. To solve this trajectory optimization problem, the bank angle is parametrized with respect to energy e and the angle of attack is obtained using load factor and heat rate constraints.

Bank angle Parametrization

The control variable, bank angle, is considered to be a linear function of current energy e as defined in Lu (2014), based on piecewise linear approximation. Its magnitude is calculated from Eq. (17)

$$|\sigma(e)| = \sigma_0 + \frac{e - e_0}{e_f - e_0}(\sigma_f - \sigma_0) \tag{17}$$

where e_0 and e_f = energies at entry interface and terminal points, respectively. $\sigma_0 \geq 0$ is the parameter to be found that minimizes the given objective function. σ_f is the predefined terminal bank angle. $\sigma_f = 60°$ is chosen for the simulations. The sign of the bank angle is obtained from a bank reversal logic as described by Shen and Lu (2004). The main aim of bank reversal logic is to reduce the heading offset $\Delta\psi$ of the vehicle.

Converting the Path Constraints to Bounds on Angle of Attack

This subsection describes a methodology that converts the path constraints, heat rate, dynamic pressure, and load factor to allowable limits on the angle of attack α.

Angle of Attack Corresponding to Heat Rate Constraint

The atmospheric density that is required to make the vehicle experience the specified maximum heat rate $\dot{Q}_{max}$ is denoted as $\rho_Q(V)$ and is given by

$$\rho_Q(V) = \frac{\dot{Q}_{max}^2}{k_q^2 V^{6.3} V_{scale}^{6.3}} \tag{18}$$

By using the above expression for density, the normalized drag acceleration that is needed to satisfy this $\dot{Q}_{max}$ is calculated and is given below

$$D_{\dot{Q}} = \frac{\dot{Q}_{max}^2 S_{ref} C_{DQ}}{2 m g_0 k_q^2 V^{4.3} V_{scale}^{4.3}} \tag{19}$$

where C_{DQ} = coefficient of drag corresponding to $\dot{Q}_{max}$ and $k_q = 9.4369 \times 10^{-5}$ as given in Eq. (13). At any given instant, the condition on current drag acceleration, D, required to satisfy the heat rate constraint is that

$$D \leq D_{\dot{Q}} \tag{20}$$

In the above equation, by considering only the equality constraint and on substituting the expression for current drag D given in Eq. (9) into Eq. (20), the coefficient of drag, C_{DQ}, needed to satisfy the heat rate limit is found as given below

$$C_{DQ}(\alpha_Q, M) = \frac{\rho C_D k_q^2 V^{6.3} V_{scale}^{6.3}}{\dot{Q}_{max}^2} = \frac{\rho C_D}{\rho_Q} \tag{21}$$

where C_D is coefficient of drag corresponding to current drag acceleration D. In the above expression, C_{DQ} is a function of angle of attack, α_Q, and Mach number. On obtaining C_{DQ} from Eq. (21), the angle of attack α_Q for a specified heat rate constraint is calculated at any given instant. To satisfy the heat rate constraint, the angle of attack α at any given instant should satisfy the following condition

$$\alpha \geq \alpha_Q \tag{22}$$

Angle of Attack Corresponding to Dynamic Pressure Constraint

By carrying out a similar procedure, the density, ρ_q, required to make the vehicle fly at a specified dynamic pressure limit q_{max} is

$$\rho_q = \frac{2 q_{max}}{V^2 V_{scale}^2} \tag{23}$$

The normalized drag acceleration, D_q, is obtained using density ρ_q given by

$$D_q = \frac{q_{max} S_{ref} C_{Dq}}{m g_0} \tag{24}$$

At any instant, the condition on current drag acceleration D to satisfy q_{max} is that

$$D \leq D_q \tag{25}$$

On substituting the expression for current drag, D, given in Eq. (9) into Eq. (25), by considering the equality condition in the above equation and finding out coefficient of drag, C_{Dq}, results in Eq. (26) as given below

$$C_{Dq}(\alpha_q, M) = \frac{\rho C_D V^2 V_{scale}^2}{2 q_{max}} = \frac{\rho C_D}{\rho_q} \tag{26}$$

The angle of attack, α_q, needed to make the vehicle fly at q_{max} is obtained using the coefficient of drag, C_{Dq}, given in Eq. (26). The angle of attack, α, at any instant should then satisfy the following relation given in Eq. (27) to satisfy the dynamic pressure constraint

$$\alpha \geq \alpha_q \tag{27}$$

Angle of Attack Corresponding to Load Factor Constraint

By following the similar approach, the angle of attack, α_l, required to make the vehicle fly at a specified load factor, a_{max}, is obtained using the coefficient of drag, C_{Da}, given in Eq. (28)

$$C_{Da}(\alpha_l, M) = \frac{\rho C_D}{\rho_a} \tag{28}$$

The angle of attack, α, at any instant should then satisfy the following equation to satisfy the load factor constraint

$$\alpha \geq \alpha_l \tag{29}$$

It is noted that the drag coefficient is normally a nonlinear function of the angle of attack and in the case of a CAV-H vehicle, upon solving, two values of the angle of attack are obtained for a given drag coefficient and Mach number. One of these values corresponds to a negative angle of attack which is out of the angle of attack bounds considered in this paper, and, therefore, it is ignored. Only the positive angle of attack is to be considered. Therefore, the commanded angle of attack, α, profile should always be above the α_Q, α_l, and α_q profiles as given below

$$\alpha \geq max\{\alpha_Q, \alpha_l, \alpha_q\} \tag{30}$$

Eq. (30) at any instant provides the lower limit on the angle of attack which can be used to satisfy the path constraints.

Angle of Attack Commands

The angle of attack required to make the vehicle fly at load factor a_{max} is also obtained by solving Eq. (31)

$$\frac{\rho V^2 V_{scale}^2 S_{ref}\sqrt{C_{La}^2 + C_{Da}^2}}{2mg_0} = a_{max} \tag{31}$$

where $C_{La}(\alpha_a, M)$ and $C_{Da}(\alpha_a, M)$ are coefficients of lift and drag, respectively, which are functions of the angle of attack and Mach number corresponding to the given a_{max}. At every instant, Eq. (31) can be solved using the fsolve command in MATLAB for finding α_a which will make the entry trajectory satisfy the specified a_{max}.

Objective Function

In the PIO based trajectory optimization methodology, two approaches for modulating the angle of attack are considered. In both the cases, the decision variable to be found is bank angle. The objective function for both the cases is given below: the trajectory optimization problem is stated as, to find the decision variables σ_0 that minimize terminal error in range-to-go, altitude, and velocity as described in J

$$MinJ = \frac{|s(e_f) - s^*| \times R_0}{1.852 \times 10^5} + \frac{|r(e_f) - r^*| \times R0}{1000} + \frac{|V(e_f) - V^*| \times V_{scale}}{100} \tag{32}$$

subject to dynamic equations, Eqs. (13) and (14).

In the objective function, "*" indicates the desired terminal states as defined by the TAEM phase. The terms in the objective function in Eq. (32) are dimensional, the range-to-go term is in nmi, the radial distance term is in km and velocity in m/s, and they are multiplied with some weights to bring them to the same order in magnitude.

Procedure for Calculating Angle of Attack

Angle of Attack in Case 1

The angle of attack, α, command at any instant is obtained by solving Eq. (31) for a specified upper bound on load factor a_{max}. The following is the logic for obtaining the commanded angle of attack, α, at every instant:

- Find the intermediate angle of attack variable, α_1, using the equation given below

$$\alpha_1 = min\{\alpha_{max}, \alpha_a\} \tag{33}$$

- Using α_1, find the required angle of attack command α

$$\alpha = max\{\alpha_{min}, \alpha_1\} \tag{34}$$

where α_{max} and α_{min} = specified upper and lower bounds on the angle of attack for a given vehicle. In this case, the angle of attack commands are obtained using above-mentioned logic, and the bank angle that minimizes the objective function is determined using the PIO algorithm.

Angle of Attack in Case 2

The angle of attack profile generated in Case 1 can lead to errors in the terminal altitude for certain specified load factor upper bounds. Due to the angle of attack profile obtained in Case 1, the resulting peak heat rate is much lesser than the specified peak heat rate. This indicates that excess control effort is being used, and to overcome these issues a different approach of finding angle of attack profiles is presented in Case 2.

In this case, the commanded angle of attack, α, is initially derived using the heat rate constraint limit using Eq. (21) and subsequently uses the load factor constraint equation [Eq. (31)]. The logic for generating α at every instant is given as follows:

- At the first instant, an initial guess for the angle of attack which is within its bounds is chosen. By using that initial guess, the coefficient of drag, C_D, is calculated.
- This coefficient of drag, C_D, is used to calculate the coefficient of drag, C_{DQ}, corresponding to the heat rate constraint using Eq. (21).
- Using the calculated C_{DQ}, the angle of attack, α_Q, is calculated for a given Mach number

$$\alpha_i = min\{\alpha_{max}, \alpha_Q\} \tag{35}$$

$$\alpha = max\{\alpha_{min}, \alpha_i\} \tag{36}$$

- This α, along with the bank angle σ are used to integrate the equations of motion.
- In the next instant, the angle of attack at the previous instant is used to calculate the coefficient of drag, C_D. On using this C_{DQ}, α_Q is subsequently calculated. This process of calculating angle of attack commands using the heat rate constraint is repeated until the vehicle attains certain Mach number $Mach_{shift}$.
- After attaining a particular $Mach_{shift}$, the angle of attack is obtained by solving the load factor constraint given in Eq. (31) as described in Case 1

$$\alpha_1 = min\{\alpha_{max}, \alpha_a\} \tag{37}$$

$$\alpha = max\{\alpha_{min}, \alpha_1\} \tag{38}$$

This shift in the angle of attack from α_Q to α_a should be smooth considering the angle of attack rate and acceleration limits. Using this approach of modulating the angle of attack, the peak heat rate achieved in this case is nearly the same as the desired peak heat rate $\dot{Q}_{max}$. As the longitudinal dynamics are coupled with the angle of attack, shifting it from α_Q to α_a at the appropriate Mach number, $Mach_{shift}$, that affects terminal velocity, which in return affects terminal altitude. Therefore, the choice of Mach number, $Mach_{shift}$, plays a significant role in achieving the desired final altitude. This switch over helps in better management of the path constraints such as the heat rate and load factor. Few subcases with different choices of $Mach_{shift}$ are discussed in the "Simulation Results" section. Though using the α_Q in the initial phase of entry reduces the control effort, it can make the load factor constraint active which may lead to the violation of the heat rate constraint. The steps involved in calculating α for this case are discussed in Fig. 2.

Pigeon Inspired Optimization

The PIO algorithm has successfully solved the entry trajectory optimization problem, and it converges in less number of iterations compared with PSO and gravitational search algorithm (GSA) as shown in Sushnigdha and Joshi (2017). Pigeons can locate themselves relative to their destination by being able to sense the magnetic field of the Earth. This process is termed as map operator. They adjust their flying direction using altitude of the Sun, which is regarded as the compass operator. The basic algorithm is evolved as follows.

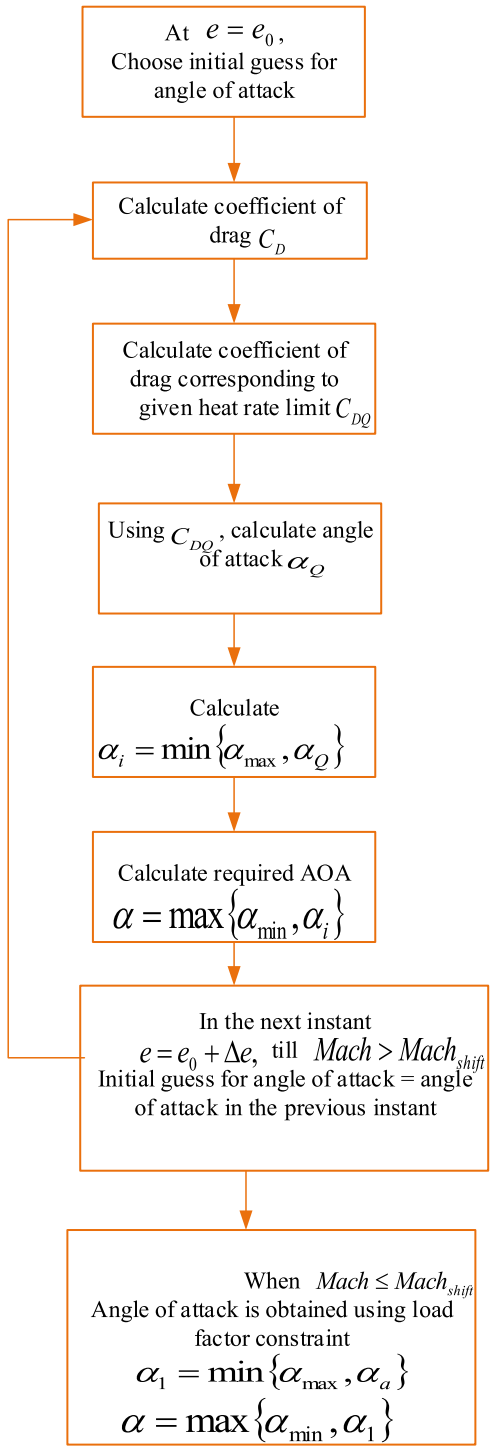

Fig. 2. Steps involved for finding angle of attack in Case 2.

Let the total population of the pigeons be N. Set the maximum number of iterations to k_{max}. Define the dimension of the problem based on the number of decision variables to be found. Let D denote the dimension of the problem. Define the search range for each dimension. The initial set of pigeons is randomly generated in the given search range. The position of the pigeon i is given by Eq. (39)

$$X_i = [x_{i1}, x_{i2}, \ldots, x_{iD}] \quad where\ i = 1, 2, 3 \ldots N \tag{39}$$

The velocity of the pigeon i is given by Eq. (40)

$$V_i = [v_{i1}, v_{i2}, \ldots, v_{iD}] \quad where\ i = 1, 2, 3 \ldots N \tag{40}$$

Each pigeons position represents a possible solution and corresponds to an objective function given in Eq. (32). In this operator, all the pigeons adjust their position and will try to follow the pigeon that corresponds to the best objective function value, i.e., minimum objective function. The position and velocities of the pigeons are updated in each iteration k as per the following update logic

$$V_i(k) = V_i(k-1).e^{-Rk} + rand.(G(k-1) - X_i(k-1)) \tag{41}$$

$$X_i(k) = X_i(k-1) + V_i(k) \tag{42}$$

where $G(k-1)$ = position of the pigeon corresponding to the best objective function achieved so far. *rand* is a random number in [0,1]. R = map and compass operator which is treated to be a constant in this study. The term $V_i(k-1).e^{-Rk}$ gives the pigeons former flying direction. As pigeons approach their destination, they use a landmark operator. Few pigeons can identify the landmarks and can fly directly to their destinations. The remaining pigeons follow them and reach the destination.

Let k_c be the iteration number that indicates the shift in the operator. k_c is chosen to be 75% of k_{max} as per (Duan and Qjao 2014). When the current iteration k becomes equal to k_c, the landmark operator is initiated. In this operator, half of the pigeons with positions nearer to $G(k-1)$ are selected. The center of these pigeons is found using Eq. (43)

$$X_c(k) = \frac{\sum_{N_p(k)} X_i(k-1).fitness(X_i(k-1))}{N_p(k) \sum_{N_p(k)} fitness(X_i(k-1))} \tag{43}$$

where $fitness()$ = objective function value corresponding to the given position of the pigeon, and N_p is the current reduced population as given below

$$N_p(k) = \frac{N_p(k-1)}{2} \tag{44}$$

Using $X_c(k)$, the positions of the pigeons is updated as follows

$$X_i(k) = X_i(k-1) + rand.[X_c(k) - X_i(k-1)] \tag{45}$$

In the landmark operator, pigeons that are not familiar with the landmarks, adjust their positions and follow the center of the pigeons that are familiar with the landmarks. Finally, at the end of iterations, the pigeon corresponding to the minimum objective function value will be the pigeon with the best position. The PIO algorithm as applied to the current problem with equilibrium glide constraint is presented in the next subsection.

Comparison of PIO with PSO Algorithm

- The map and compass operator of the PIO algorithm has an exponential e^{-Rk} weighting factor associated with the previous velocity of pigeons as given in Eq. (41), whereas the PSO algorithm has a weight w which is either constant or linearly varying. As a result of this difference, with the increase in the number of iterations, this weighing factor in the PIO reduces the influence of the pigeons' previous velocity on the current velocity and hence allows the PIO algorithm to converge at a faster rate to the optimal value when compared with the PSO algorithm.
- In the landmark operator of the PIO algorithm, the update of the pigeons' position is performed by considering the fitness values

of each pigeon, whereas the PSO algorithm does not consider the quality of its particles.
- In the updated equations, the PSO algorithm requires usage of the best position that the particle has achieved so far. Therefore, it requires memory, whereas the PIO algorithm is independent of this aspect. Both the algorithms require memory to keep track of the global best position.

Incorporating Quasi Equilibrium Glide Constraint

The entry trajectory of a CAV-H vehicle exhibits oscillations as seen in the simulation results of Sushnigdha and Joshi (2017), and these oscillations result in peak heat rates and g-loads. This section presents a methodology to eliminate these oscillations by utilizing the slope of the altitude limit curve corresponding to a equilibrium glide condition in velocity-altitude space and by modulating the vertical component of lift accordingly so that the vehicle satisfies this constraint. This equilibrium glide condition is obtained by making $\dot{\gamma} = 0$ in Eq. (5) and ignoring the terms related to the rotation of the Earth. The obtained equation is further simplified by choosing σ to be 0, $r \approx 1$, and $\gamma \approx 0$. In this simplified equation, the altitude required to fly at the equilibrium glide condition for a given velocity is obtained by substituting the lift acceleration expression Eq. (8) and by expressing density as a function of altitude using the exponential density model. The resulting relationship between altitude and velocity is given below

$$r_{eq} = 1 + \frac{1}{\beta}\log\left(\frac{V_{scale}^2 V^2 \rho_0 S_{ref} C_L}{2mg_0(1-V^2)}\right) \tag{46}$$

where $\beta = 920$ is nondimensional scale height which is normalized with the radius of the Earth. Eq. (46), gives the altitude required to satisfy the equilibrium glide condition at any given velocity. On differentiating the above equation with respect to velocity and equating it with the ratio of Eqs. (1) and (2), results in a equation using the flight-path angle required to fly the vehicle at equilibrium glide condition can be obtained as

$$sin\gamma_{QEGC} = \frac{-D}{\beta V^3(1-V^2) + (1/r^2)} \tag{47}$$

The above expression for γ_{QEGC} can be used to find the altitude variation with respect to energy $\frac{dr_{QEGC}}{de} = \frac{sin\gamma_{QEGC}}{D}$ required to fly the vehicle in QEGC. The current variation of altitude with respect to energy is given by $\frac{dr}{de} = \frac{sin\gamma}{D}$. The vertical component of lift force is modulated by using the altitude compensation term $k(\frac{dr}{de} - \frac{dr_{QEGC}}{de})$ as described in Lu (2014), given in Eq. (48)

$$L\cos\sigma_{cmd} = L\cos\sigma_{base} - k_2\left(\frac{dr}{de} - \frac{dr_{QEGC}}{de}\right) \tag{48}$$

where σ_{base} = bank angle at the current energy obtained using Eq. (17). $k_2 = 10$ is a constant gain used for simulations. Bank angle σ_{cmd} is used to integrate the equations of motion, and the objective function is evaluated. This bank angle σ_{cmd} eliminates the oscillations observed in the altitude profile of high L/D vehicles.

The decision variable to be found using the PIO algorithm is the bank angle σ_0 as in Eq. (17). This bank angle σ_0 is utilized to calculate the bank angle σ_{base} at each instant from Eq. (17). At each instant, this bank angle is further modified to σ_{cmd} using Eq. (48) to satisfy the equilibrium glide constraint. The angle of attack control commands at each instant are obtained as discussed in the previous section. With these two control variables, equations of motion are integrated from the initial energy e_0 to e_f. After attaining the final energy e_f, the objective function is evaluated. The flowchart of the PIO based trajectory optimization algorithm is given in Fig. 3.

Simulation Results

In this section, simulation results are demonstrated for the CAV-H vehicle. The PIO algorithm is used to find the bank angle that minimizes the terminal range-to-go error and that ensures the equilibrium glide condition. Another control variable, angle of attack, is modulated to satisfy heat rate and load factor constraints. Thus, the obtained entry trajectory satisfies the path and terminal constraints. The initial conditions and terminal conditions used for both the cases are given in Sushnigdha and Joshi (2017). Various cases with $Mach_{shift} = 20, 16, 10$ are considered as part of Case 2. The parameters required for simulating the PIO algorithm are set as $N = 10$, $k_{max} = 20$, $k_c = 14$, and $R = 0.2$. The dimension of the problem is $D = 1$, as bank angle, σ_0 is the parameter to be found. For comparing the performance of the PIO algorithm with the PSO algorithm, the same parameters such as population size and maximum number of iterations are chosen. Additional parameters $c_1 = 1.4$, $c_2 = 2.6$, $w_{max} = 1$, and $w_{min=0.4}$, linearly decreasing weighing factor w are considered in the PSO algorithm. In both the algorithms, the range of search space for σ_0 is given as $|\sigma_{min}| = 0^{\circ}$ and $|\sigma_{max}| = 89^{\circ}$. The upper and lower bounds of the angle of attack are considered to be 20° and 10°, respectively. The entry corridor is obtained using constraint limits on heat rate $\dot{Q}_{max} = 6\,\mathrm{MW/m^2}$, load factor $a_{max} = 2$ g, and dynamic pressure $q_{max} = 6 \times 10^4$ Pa. The additional constraints on the angle of attack rate 4°/s and acceleration 8°/s are considered in the simulations.

The values of bank angle σ_0 obtained using the PIO are 58.89°, 59.684°, 65.08°, and 67.563° in Case 1, Case 2 with $Mach_{shift} = 20$ and remaining subcases, respectively. It is observed that the PIO algorithm converges to the minimum objective function value in nine iterations which indicates that the solution has converged even before the landmark operator of the PIO algorithm is initiated.

The performance of the PIO is compared with PSO algorithms for Case 1; each algorithm is executed five times, and the results are tabulated in Table 1. It is evident from Table 1 and Fig. 4 that the PIO algorithm has taken fewer iterations to converge to the minimum objective function value compared with the PSO algorithm. It is seen that the PIO algorithm has converged to the mean objective function value of 0.3783 with a standard deviation of 4.1593×10^{-4} which is less than the converged value of the PSO algorithm. The average iterations taken by the PIO algorithm to converge to the obtained minimum objective function value is 11.8 with a standard deviation of 4.1473 which are less than the average iterations taken by the PSO algorithm. This faster convergence of the PIO algorithm could be attributed to the exponential weighing factor present in the velocity update equation.

The path constraints, load factor, and heat rate constraints are strictly satisfied in Case 1 and in Case 2 with $Mach_{shift} = 20$ as shown in Figs. 5 and 6, respectively. The constraint on final range-to-go is satisfied in all the cases, whereas an error of 350 m is observed in the final altitude of Case 1. This error in the final altitude might be higher or lower according to the specified load factor constraint a_{max}. In Case 1, as the vehicle is flying at a high angle of attack of 20°, the peak heat rate experienced by the vehicle is as low as $3.83 \times 10^6\ \mathrm{W/m^2}$ which is much lower than the specified $\dot{Q}_{max}$ as shown in Fig. 6. In the second case with $Mach_{shift} = 20$, initially, the vehicle flies at an angle of attack derived from the heat rate constraint. Therefore, theobserved peak heat rate $6.06 \times 10^6\ \mathrm{W/m^2}$ as seen in Fig. 6 is almost the same as $\dot{Q}_{max}$. This method of flying at an angle of attack derived from

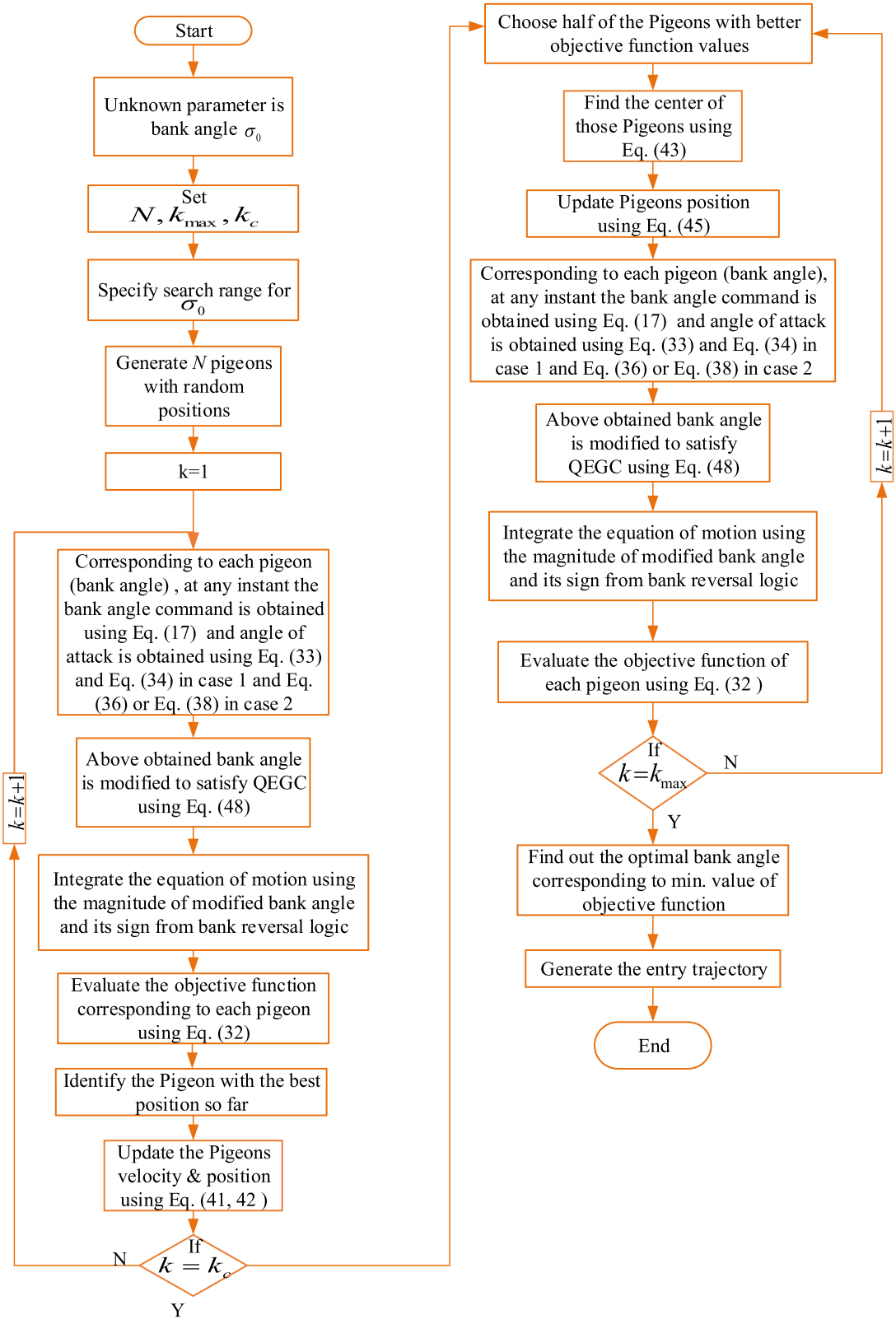

Fig. 3. Flowchart of the PIO algorithm for solving entry trajectory optimization problem.

Table 1. Statistical performance comparison of PIO and PSO algorithms with five runs for Case 1

Algorithms	Mean iterations	Standard of iterations	Mean objective function value	Standard of objective function value
PIO	11.8000	4.1473	0.3783	4.1593×10^{-4}
PSO	12.6000	5.94	0.4530	0.0415

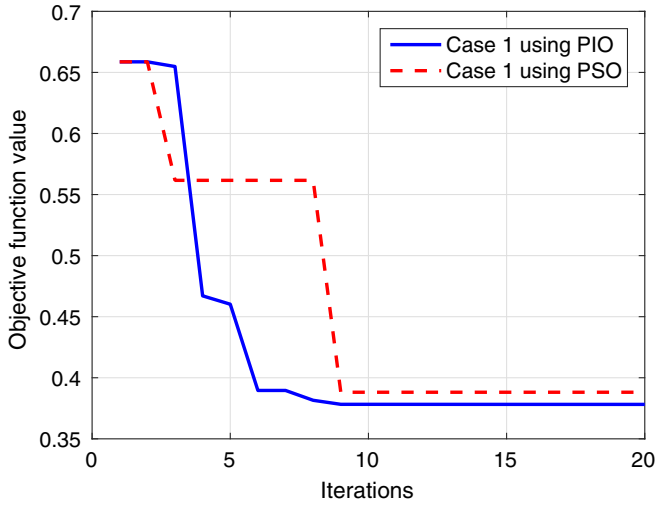

Fig. 4. Objective function value corresponding to each iteration.

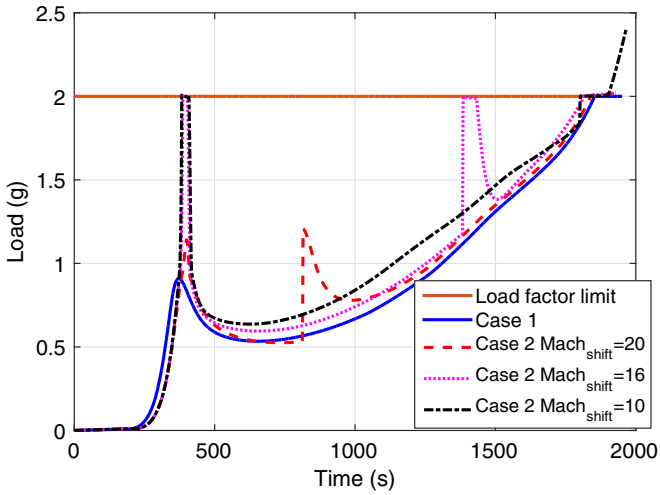

Fig. 5. Variation of load factor with time.

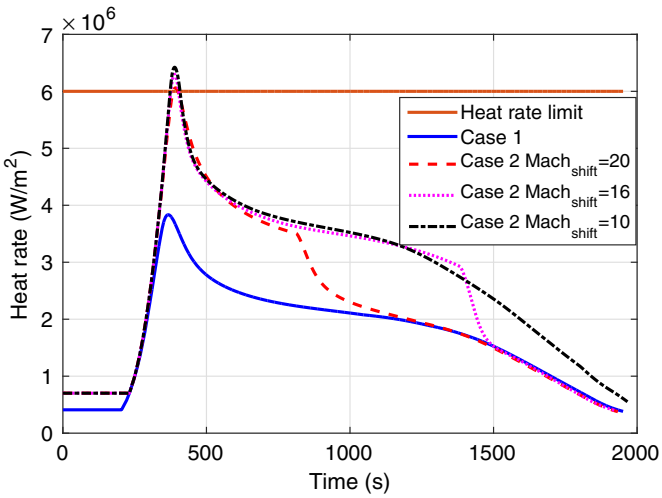

Fig. 6. Heat rate variation with time.

the given heat rate constraint and subsequently shifting to an angle of attack derived from the load factor constraint reduces the control effort and the error in terminal altitude to some extent. The error in terminal altitude for this case is 180 m which is less than Case 1. In Case 2 with $Mach_{shift} = 16$, the load factor constraint becomes active in the initial phase of re-entry as shown in Fig. 5. Therefore, the angle of attack α_a is considered, which led to the violation of the heat rate constraint. The peak heat rate of 6.29×10^6 W/m^2 is observed in Fig. 6, whereas the peak load factor is satisfied in Fig. 5. The error in terminal altitude is about 610 m. Similar to this case, Case 2 with $Mach_{shift} = 10$ also has violated the heat rate constraint as seen in Fig. 6. The error in terminal altitude is 4.57 km, which is not desired. Towards the end of entry phase, ithe load factor constraint is also violated because the angle of attack required to maintain 2 g is less than its specified lower bound 10°. From the above considered cases, it is clear that constraint limits have to be compromised, i.e., by increasing/decreasing their values, the entry trajectory will be able to satisfy both the path and terminal constraints. A careful choice of $Mach_{shift}$ can also enable entry trajectory to satisfy all the constraints. Overall, Case 2 has a lower angle of attack control effort as observed from Fig. 7 compared with Case 1. Case 2 with $Mach_{shift} = 20$ also has less final altitude error compared with other cases, and it also satisfies all the path constraints.

Fig. 8 shows the bank angle profile for all the cases. The bank angle magnitude is zero initially until the vehicle attains sufficient dynamic pressure. After this phase, the magnitude of the bank angle decreases suddenly and gradually increases to make the vehicle satisfy QEGC. The sign of the bank angle changes based on the heading error corridor.

The angle of attack profiles for all the cases is given in Fig. 7. In Case 1, the initial angle of attack obtained using the load factor constraint is greater than the specified upper bound of the angle of attack, i.e., 20°. Therefore, the angle of attack is at 20° until the load factor constraint is active, and subsequently the angle of attack gradually decreases to make the vehicle fly at 2 g. In Case 2 with $Mach_{shift} = 20$, an angle of attack is obtained from the heat rate constraint initially until $Mach > 20$. In the beginning of the entry trajectory, the angle of attack demanded by the heat rate constraint is less than the specified lower bound of the angle of attack; therefore, the angle of attack is maintained at 10°. Once the vehicle attains $Mach < 20$, the angle of attack gradually increases

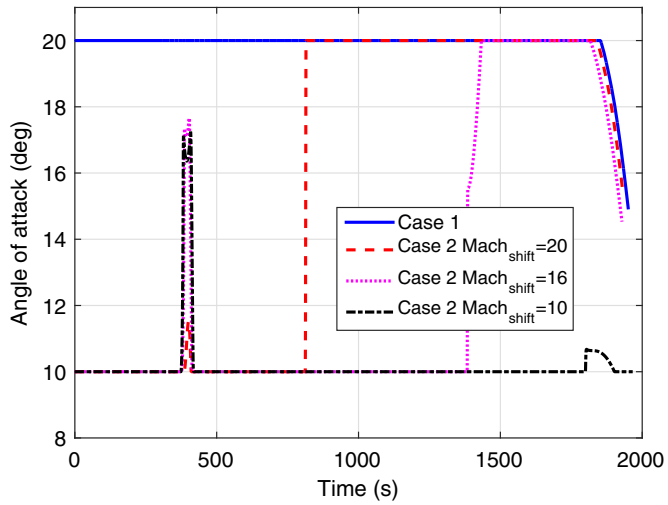

Fig. 7. Angle of attack profile.

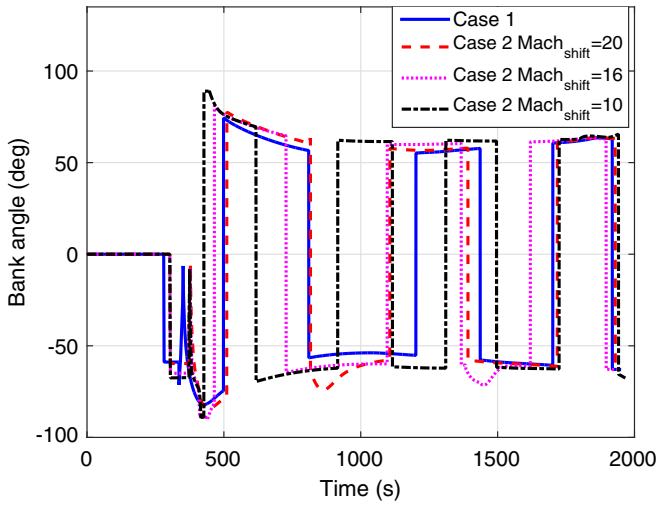

Fig. 8. Bank angle profile.

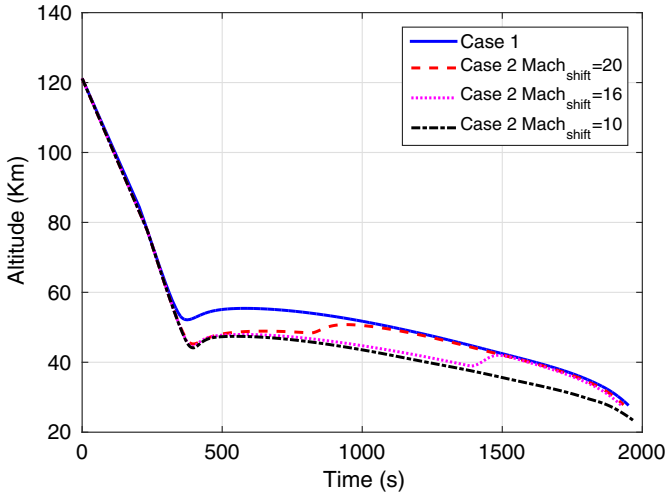

Fig. 10. Variation of altitude with time.

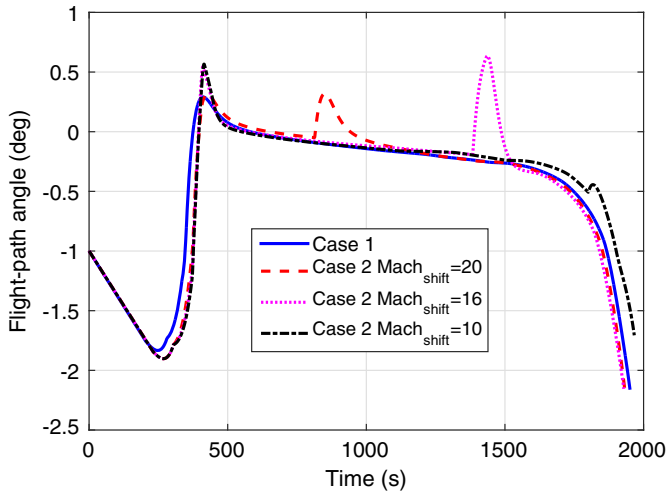

Fig. 9. Variation of flight-path angle with time.

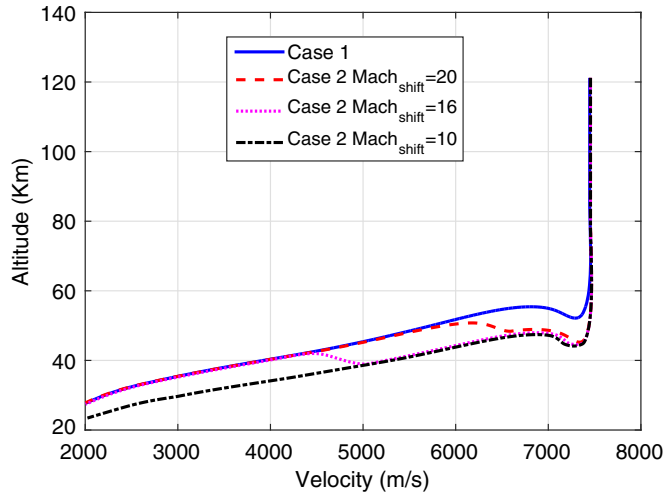

Fig. 11. Variation of altitude with velocity.

to 20° until the load factor constraint becomes active. A gradual increase in the flight-path angle is observed in Fig. 9, whenever there is a shift in the angle of attack at different Mach numbers. This makes the vehicle fly at higher altitude after Mach < 20, Mach < 16 as seen in Fig. 10. The variation of altitude with velocity is shown in Fig. 11. The terminal constraint on range-to-go is satisfied in all the cases. The variation of dynamic pressure is seen in Fig. 12. Whenever the load factor constraint is satisfied, the constraint on dynamic pressure is implicitly satisfied, except for the last case where $Mach_{shift} = 10$, the load factor and dynamic pressure constraints are violated towards the end of the trajectory.

Fig. 13 shows that the angle of attack profile corresponding to Case 2 with $Mach_{shift} = 20$ lies above or on the profiles α_Q and α_q. It is also observed from the Fig. 13, that the angle of attack obtained from the heat rate constraint is positive and active until 1,100 s, after which, the angle of attack obtained from the heat rate constraint is 10° as per Eq. (36) until the Mach number $Mach_{shift}$ is attained by the vehicle. After which, the angle of attack is derived from the load factor constraint.

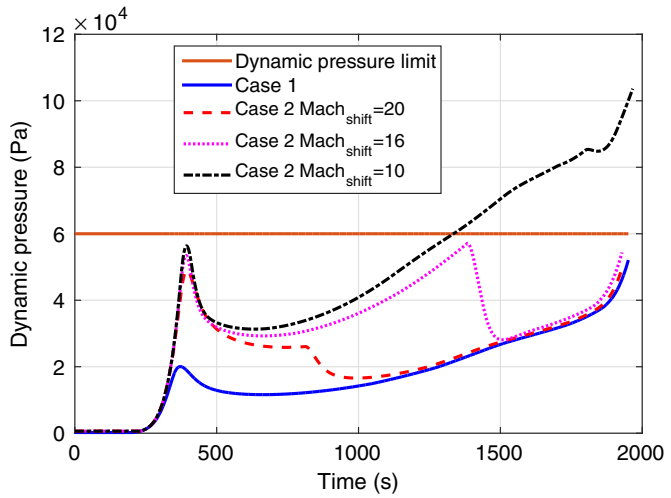

Fig. 12. Variation of dynamic pressure with time.

J. Aerosp. Eng., 2018, 31(6): 04018104

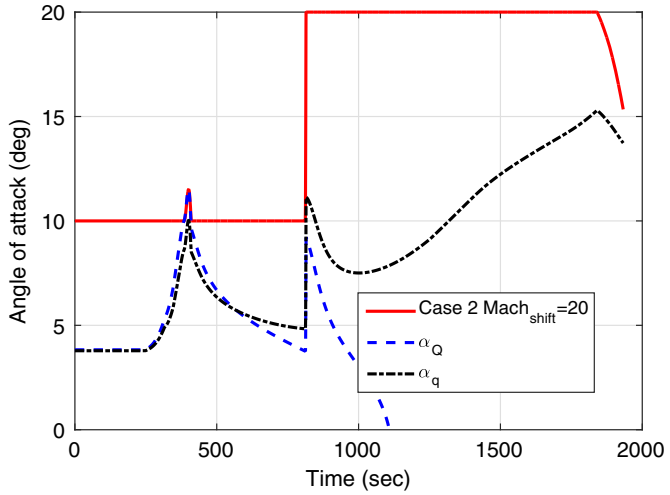

Fig. 13. Angle of attack profile with constraint limits.

Conclusion

The entry trajectory obtained using the PIO algorithm with proposed schemes of generating angle of attack commands satisfies the path constraints and the terminal range-to-go constraint accurately. In Case 1, the vehicle flies at a high angle of attack, and the peak heat rate has reduced considerably which eventually led to usage of more control effort and can also lead to a large error in terminal altitude for some specified load factor constraint limit a_{max}. In Case 2, angle of attack commands derived from the heat rate constraint is used until the vehicle attains $Mach_{shift} = 20$ after which angle of attack commands derived using the load factor constraint are used in generating the entry trajectory. The obtained entry trajectory has satisfied the path and terminal constraints accurately with reduced control effort in the angle of attack as compared with Case 1. Various subcases with different $Mach_{shift}$ are considered, it is observed that flying with an angle of attack derived from the heat rate constraint has also led to increasing g-load in the initial phase of the entry trajectory, and a suitable choice of $Mach_{shift}$ can reduce the error in terminal altitude. Though Case 2 reduces the angle of attack control effort, the load factor constraint becomes active in the initial descent. Hence, a trade off between control effort requirement and limits on g-loads should be made based on the mission requirements. In both cases, the bank angle is modulated to achieve the desired range-to-go. The two methods proposed in this paper have both the angle of attack and the bank angle as the control variables, unlike many methods in the literature which modulate only the bank angle to satisfy all the path and terminal constraints. This paper also derives the lower bound on the angle of attack, i.e., the angle of attack control profile of an entry trajectory should always be above the angle of attack profiles obtained using the path constraints to ensure that the entry trajectory is within the entry corridor. Future work would involve deriving an analytic approach for finding $Mach_{shift}$ to achieve the desired final altitude.

References

Anon. 1976. *U.S. standard atmosphere, 1976*. Washington, DC: US Committee on Extension to the Standard Atmosphere.

Bailing, T., and Z. Qun. 2011. "Optimal guidance for reentry vehicles based on indirect legendre pseudospectral method." *Acta Astronaut.* 68 (7): 1176–1184. https://doi.org/10.1016/j.actaastro.2010.10.010.

Cai, W. W., Y. W. Zhu, L. P. Yang, and Y. W. Zhang. 2015. "Optimal guidance for hypersonic reentry using inversion and receding horizon control." *IET Control Theory Appl.* 9 (9): 1347–1355. https://doi.org/10.1049/iet-cta.2014.1155.

Duan, H., and S. Li. 2015. "Artificial bee colony-based direct collocation for reentry trajectory optimization of hypersonic vehicle." *IEEE Trans. Aerosp. Electron. Syst.* 51 (1): 615–626. https://doi.org/10.1109/TAES.2014.120654.

Duan, H., and P. Qjao. 2014. "Pigeon-inspired optimization: a new swarm intelligence optimizer for air robot path planning." *Int. J. Intell. Comput. Cybern.* 7 (1): 24–37. https://doi.org/10.1108/IJICC-02-2014-0005.

Halbe, O., R. G. Raja, and R. Padhi. 2014. "Robust reentry guidance of a reusable launch vehicle using model predictive static programming." *J. Guidance Control Dyn.* 37 (1): 134–148. https://doi.org/10.2514/1.61615.

Li, G., H. Zhang, and G. Tang. 2015. "Maneuver characteristics analysis for hypersonic glide vehicles." *Aerosp. Sci. Technol.* 43: 321–328. https://doi.org/10.1016/j.ast.2015.03.016.

Li, Z., C. Hu, C. Ding, G. Liu, and B. He. 2018. "Stochastic gradient particle swarm optimization based entry trajectory rapid planning for hypersonic glide vehicles." *Aerosp. Sci. Technol.* 76: 176–186. https://doi.org/10.1016/j.ast.2018.01.033.

Liu, X., Z. Shen, and P. Lu. 2016. "Entry trajectory optimization by second-order cone programming." *J. Guidance Control Dyn.* 39 (2): 227–241. https://doi.org/10.2514/1.G001210.

Lu, P. 2006. "Asymptotic analysis of quasi-equilibrium glide in lifting entry flight." *J. Guidance Control Dyn.* 29 (3): 662–670. https://doi.org/10.2514/1.15789.

Lu, P. 2014. "Entry guidance: A unified method." *J. Guidance Control Dyn.* 37 (3): 713–728. https://doi.org/10.2514/1.62605.

Naresh Kumar, G., M. Ikram, A. K. Sarkar, and S. E. Talole. 2018. "Hypersonic flight vehicle trajectory optimization using pattern search algorithm." *Optim. Eng.* 19 (1): 125–161. https://doi.org/10.1007/s11081-017-9367-0.

Phillips, T. H. 2003. *A common aero vehicle (CAV) model, description, and employment guide*. Peterson Air Force Base, OhioSchafer Corporation for Air Force Research Laboratory and Air Force Space Command.

Pontryagin, L. S., and V. G. Boltyanskii. 1962. *The mathematical theory of optimal processes*. New York: Wiley.

Rahimi, A., K. Dev Kumar, and H. Alighanbari. 2013. "Particle swarm optimization applied to spacecraft reentry trajectory." *J. Guidance Control Dyn.* 36 (1): 307–310. https://doi.org/10.2514/1.56387.

Shen, Z., and P. Lu. 2004. "Dynamic lateral entry guidance logic." *J. Guidance Control Dyn.* 27 (6): 949–959. https://doi.org/10.2514/1.8008.

Su, Z., and H. Wang. 2015. "A novel robust hybrid gravitational search algorithm for reusable launch vehicle approach and landing trajectory optimization." *Neurocomputing* 162: 116–127. https://doi.org/10.1016/j.neucom.2015.03.063.

Sushnigdha, G., and A. Joshi. 2017. "Re-entry trajectory design using pigeon inspired optimization." In *Proc., AIAA Atmospheric Flight Mechanics Conf.*, 1–12. Denver: AIAA.

Sushnigdha, G., and A. Joshi. 2018. "Evolutionary method based integrated guidance strategy for reentry vehicles." *Eng. Appl. Artif. Intell.* 69: 168–177. https://doi.org/10.1016/j.engappai.2017.11.010.

Vinh, N. X., A. Busemann, and R. D. Culp. 1980. *Hypersonic and planetary entry flight mechanics*. Ann Arbor, MI: University of Michigan Press.

Zhao, J., and R. Zhou. 2015a. "Particle swarm optimization applied to hypersonic reentry trajectories." *Chin. J. Aeronaut.* 28 (3): 822–831. https://doi.org/10.1016/j.cja.2015.04.007.

Zhao, J., and R. Zhou. 2015b. "Pigeon-inspired optimization applied to constrained gliding trajectories." *Nonlinear Dyn.* 82 (4): 1781–1795. https://doi.org/10.1007/s11071-015-2277-9.

Zhu, J., L. Liu, G. Tang, and W. Bao. 2015. "Highly constrained optimal gliding guidance." *Proc. Inst. Mech. Eng. Part G J. Aerosp. Eng.* 229 (12): 2321–2335. https://doi.org/10.1177/0954410015573973.